iScience, Volume *25*

Supplemental information

Role of PVAT in obesity-related cardiovascular disease through the buffering activity of ATF3

Hsiao-Fen Li, Hsin-Tzu Liu, Po-Yi Chen, Heng Lin, and Tzu-Ling Tseng

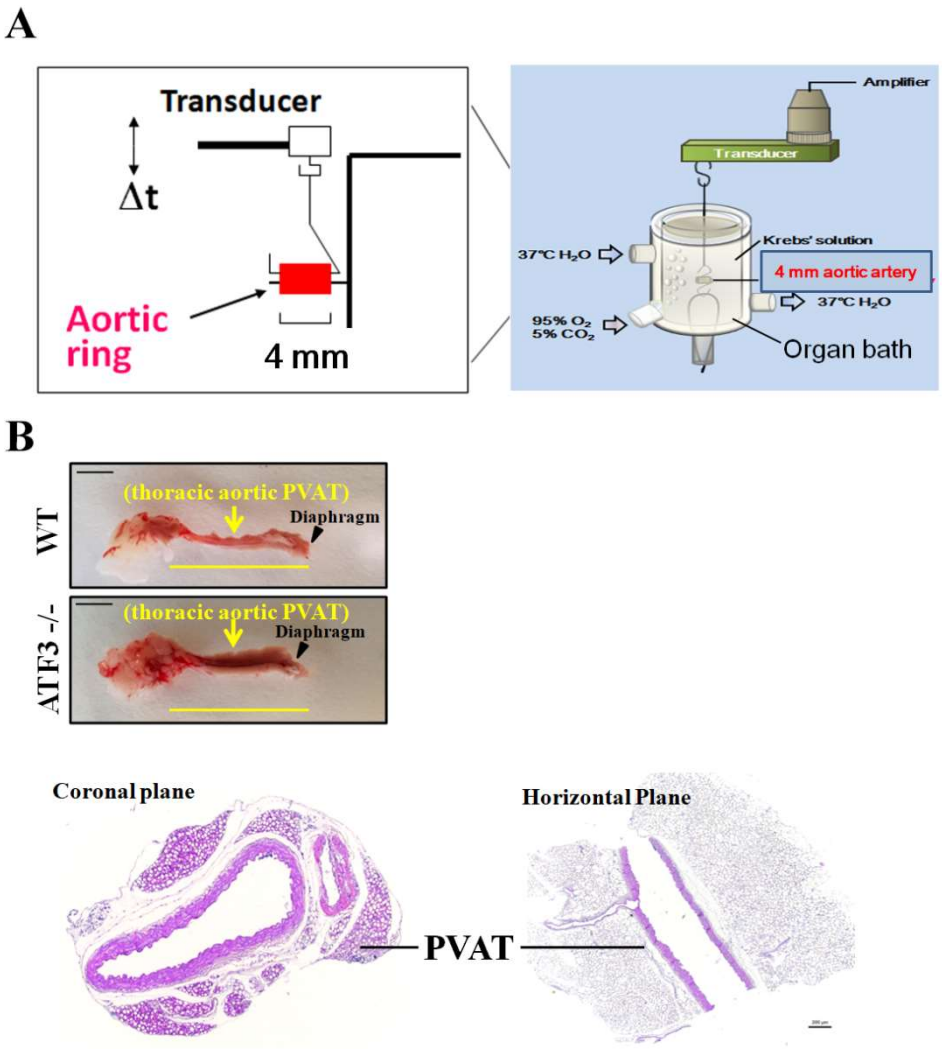

Figure S1. A simple scheme of the *in vitro* blood vessel myography system setting and aortic rings preparation, related to STAR Methods.

The 4-mm long aortic ring segment was mounted on stainless-steel rods in a tissue bath containing 10 mL Krebs solution (**A**). Tension changes were measured by an isometric transducer (FT03C; Grass Technology, West Warwick, RI, USA), as described in our previous report. The temperature of the Krebs solution equilibrated with 95% O_2 and 5% CO_2 was maintained at 37°C. Tissues were equilibrated in the Krebs solution for an initial 30 min and then mechanically stretched to a resting tension of 1 g. For comparing the effects of PVAT on vascular reactivity between WT and ATF3$^{-/-}$ mice, phenylephrine, 5-HT, and KCl concentration-response relationships for constriction were obtained by a non-cumulative technique in endothelium-denuded arteries (-EC) with or without PVAT. EC_{50} value (the concentration that produces 50% of the maximum constriction) was determined for each arterial ring. Representative image illustrating blood vessels with PVAT structure isolated from the thoracic artery of mice (**B**).

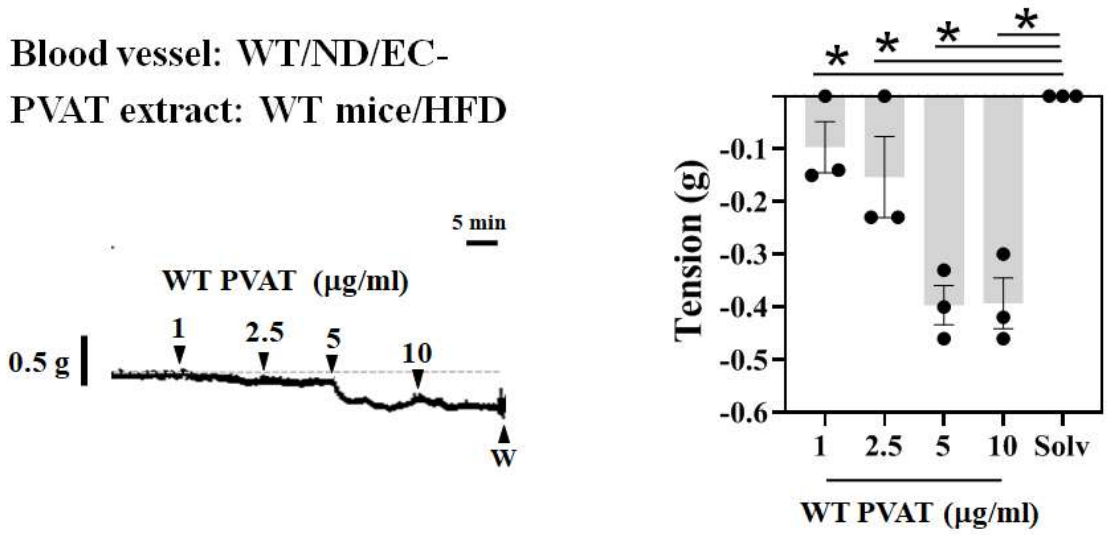

Figure S2. PVAT extracts induced resting tone vasodilatation in a concentration-dependent manner, related to Figure 1.

Concentration-dependent relaxation curves of thoracic aorta ring from wild type mice in response to thoracic aortic PVAT extract treatment of C57/B6 mice feeding a high-fat diet (HFD). The dot symbol in each column represents the number of mice examined. Number of experiments in SNP-induced relaxation= 3. A statistical comparison was performed using one-way ANOVA. Data are mean ± SEM and *p< 0.05, compared to the solvent control and single concentration application of the concentration curve. ND: normal chow; Solv: solvent (Krebs solution); W: wash.

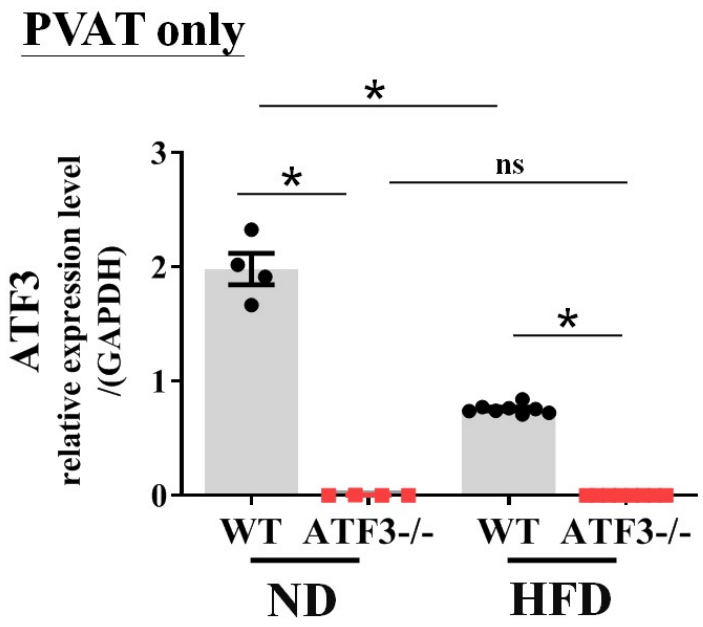

Figure S3. The expression of ATF3 in thoracic aortic PVAT fed a normal diet (ND) or high-fat diet (HFD) for 22 weeks, related to Figure 4.

Bar graphs quantify RT-PCR analysis of mRNA levels of ATF3 in thoracic aortic PVAT of WT and $ATF3^{-/-}$ mice. A statistical comparison was performed using one-way ANOVA. Data are presented as mean ± SEM; *p< 0.05 compared to the WT group in each experiment. ns: not significant. The dotted symbols in each column represent the number of mice examined.

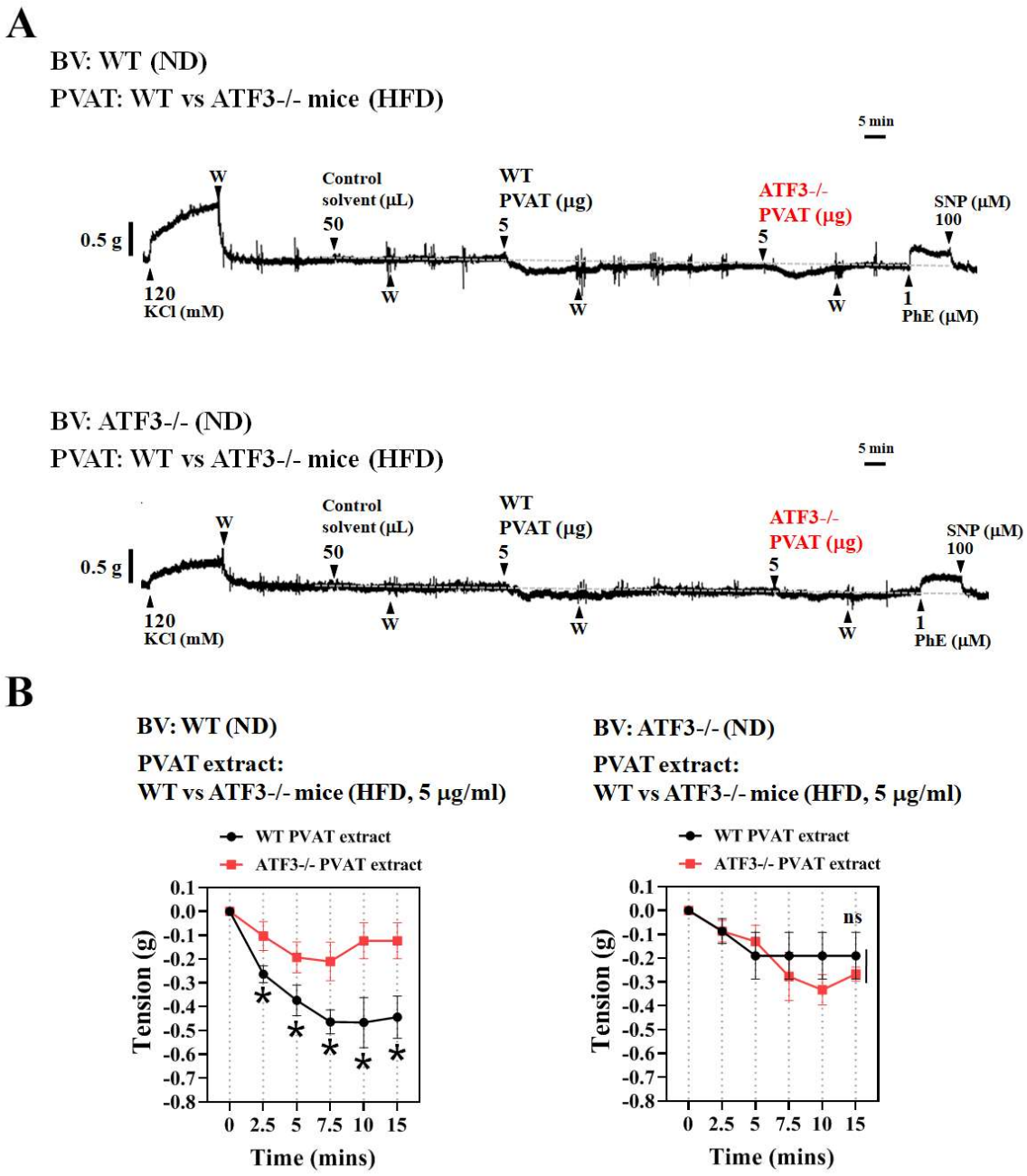

Figure S4. The vascular responses under PVAT extract switching, related to Figure 6.

Investigate the responses of the blood vessels (without PVAT) from WT or ATF3$^{-/-}$ mice feeding normal diet (ND) to PVAT extracts from WT/ATF3$^{-/-}$ mice under high-fat diet (HFD). Representative tracing showing vascular dilated responses induced by thoracic aortic PVAT extracts (5 μg/mL) from wild-type (WT) littermates and ATF3-deficient (ATF3$^{-/-}$) mice 22 weeks after HFD feeding (**A**). PVAT extract-induced time-dependent vasorelaxation is summarized in **B**. Statistical comparisons were performed using two-way ANOVA. Data are presented as mean±standard error of the mean (SEM). *p <0.05, compared to the WT group in each experiment. ns: not significant. N= 3.

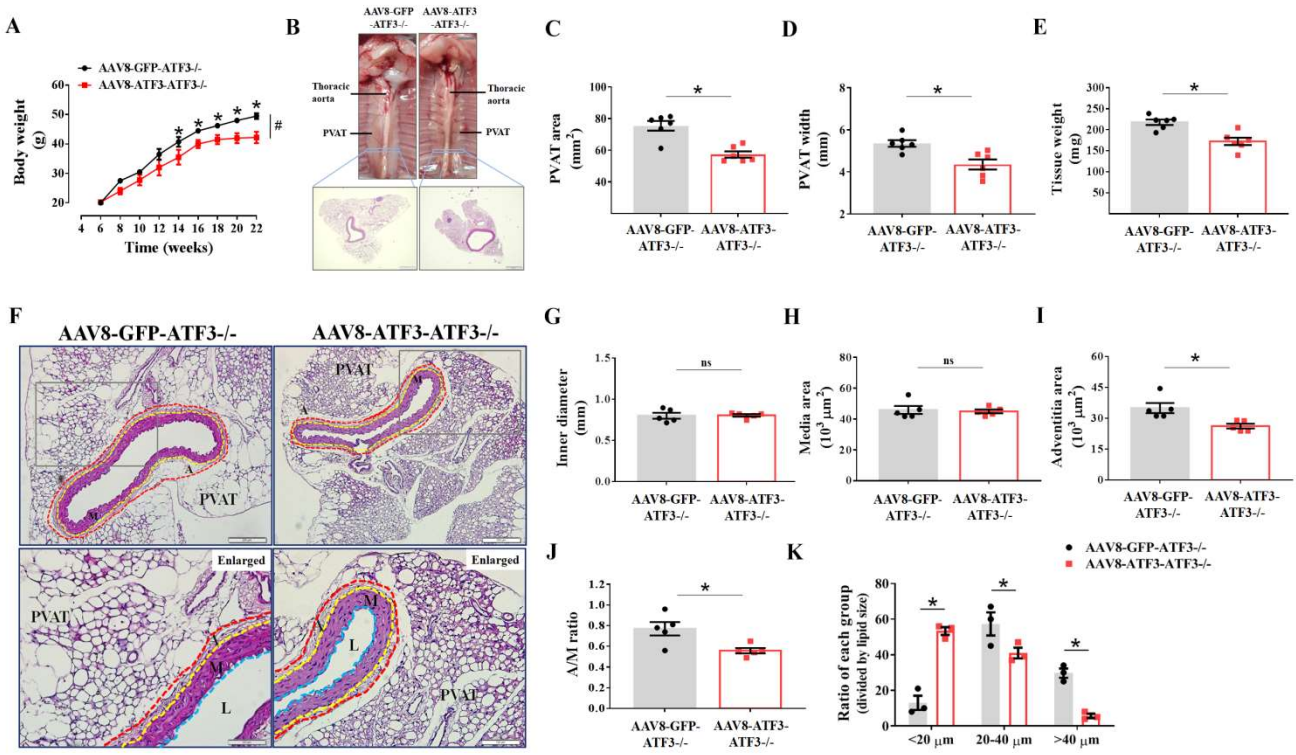

Figure S5. ATF3-deficient mice subjected to AAV-ATF3 but not AAV-GFP treatment improved pathological dysfunctions induced by obesity, related to STAR Methods.

Analysis of mice fed HFD for 22 weeks, AAV8-GFP-treated ATF3$^{-/-}$ (AAV8-GFP-ATF3$^{-/-}$), and AAV8-ATF3-treated ATF3$^{-/-}$ (AAV8-ATF3-ATF3$^{-/-}$) were examined for body weight (**A**) and microscopic differences in thoracic aortic PVAT structure (**B**) surrounding the aorta. The morphology of the thoracic aortic PVAT area (**C**), thoracic aortic PVAT width (**D**), and tissue weight (**E**) were quantified and analyzed using the ImageJ software. Representative images of the thoracic aorta stained with hematoxylin-eosin Y and magnified images of a specific area for enlarged images (**F**). The grey box shows the zoomed-in capture location of the image (**F**). Inner diameters (**G**), medial area (**H**), adventitial area (**I**), and A/M ratio (**J**) in the blood vessels of the aorta were measured and calculated using the ImageJ software. Lipid droplets were classified into three groups according to diameter: <20μm, 20–40 μm, and >40 μm, following the standard procedures (**K**). Average proportions were calculated from 100 lipid droplets in each microscopic field. Data were obtained from six fields per mouse. A, adventitia; L, lumen; M, media. Scale= 50 μm for hematoxylin and eosin Y staining. Statistical comparisons between two groups were performed by unpaired t-test (**C–J**) and one-way ANOVA in more than two groups (**K**). Figure **A** was performed by two-way ANOVA. Data are presented as mean ± standard error of the mean (SEM). *$p < 0.05$, compared to the AAV8-GFP-ATF3$^{-/-}$group in each experiment. $^{\#}$Indicatesa statistically significant difference among the sets of curves by the generalized estimating equation (GEE) analysis (**A**). The dotted symbols in each column represent the number of mice examined. ns: not significant.

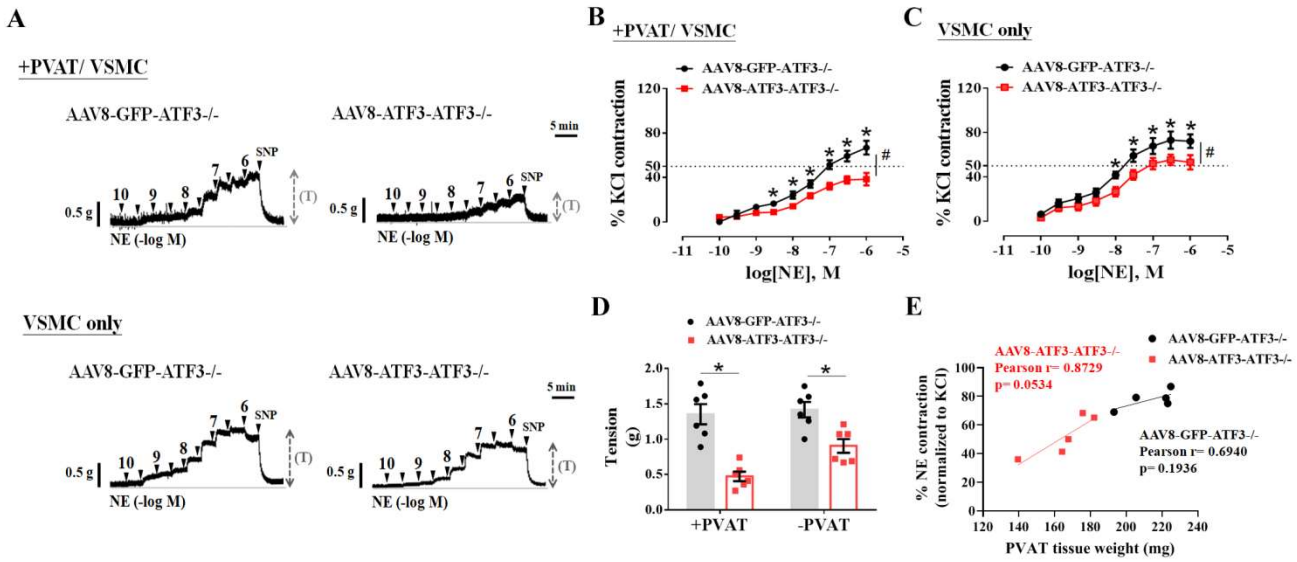

Figure S6. Adeno-associated virus 8 (AAV8)-mediated expression of ATF3 reverses the sensitivity to NE-induced vasoconstriction and over-contracting in ATF3$^{-/-}$ mice, related to STAR Methods.

Representative traces show that ATF3-deficient mice have impaired vascular reactivity restored by AAV-mediated gene transfer of ATF3 in thoracic aortic PVAT and VSMC (**A**), but have no effect on AAV8-GFP gene transfer in ATF3$^{-/-}$ mice. The NE-induced concentration-dependent constriction of arteries with or without PVAT from AAV8-GFP and AAV8-ATF3 mice is summarized and analyzed in **B** and **C**. In **D**, the tension (T) is shown as the absolute tension differential between AAV8-GFP mice and AAV8-ATF3 mice with PVAT present (+PVAT) or removed PVAT (-PVAT) but preserved vascular smooth muscle cells (VSMCs), and the levels of tension expressed in grams (g). PVAT tissue weight and percentage of NE-induced contractions were significantly improved in AAV8-ATF3-treated groups, although they did not change and were not significantly correlated in AAV8-GFP-treated ATF3$^{-/-}$ mice. Two-way ANOVA were performed in **B** and **C**. One-way ANOVA was performed in more than two groups in **D**. Data are presented as mean ± standard error of the mean (SEM). *$p < 0.05$, compared to the AAV8-GFP-ATF3$^{-/-}$group in each experiment. #There is a statistically significant difference among these sets of curves by the generalized estimating equation (GEE) analysis. The dotted symbols in each column represent the number of mice examined.

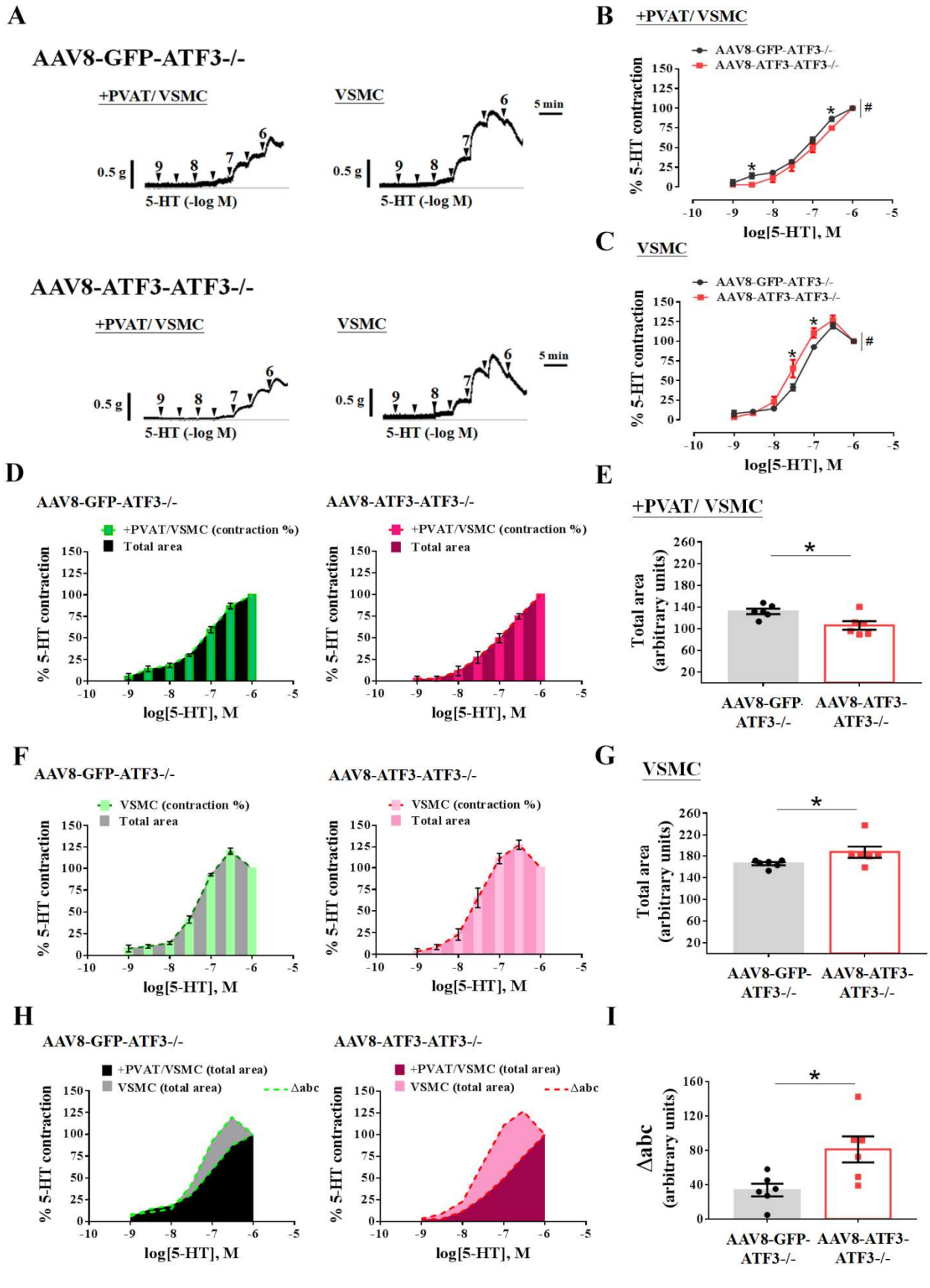
A
AAV8-GFP-ATF3-/-
+PVAT/ VSMC
VSMC
0.5 g
5 min
5-HT (-log M)
AAV8-ATF3-ATF3-/-
B
+PVAT/ VSMC
AAV8-GFP-ATF3-/-
AAV8-ATF3-ATF3-/-
% 5-HT contraction
log[5-HT], M
C
VSMC
D
AAV8-GFP-ATF3-/-
AAV8-ATF3-ATF3-/-
+PVAT/VSMC (contraction %)
Total area
E
+PVAT/ VSMC
Total area (arbitrary units)
F
VSMC (contraction %)
G
VSMC
H
+PVAT/VSMC (total area)
VSMC (total area)
Δabc
I
Δabc (arbitrary units)

Figure S7. Restoration of ATF3 gene expression improved PVAT anticontractile function in HFD-induced obese mice, related to STAR Methods.

The representative trace in **A** shows the concentration-response curve to serotonin (5-HT) in thoracic aortic PVAT (+PVAT/VSMC) and vascular smooth muscle cells (VSMC) without PVAT when AAV8-GFP or AAV8-ATF3 virus-mediated gene transfer strategy. Quantitative analysis of constriction percentage (%) of aortic rings in response to 5-HT in vessels with PVAT (**B**) or without PVAT (**C**). In **D** and **F**, contractile profiles of 5-HT-induced constriction of arteries from AAV8-GFP-ATF3$^{-/-}$ and AAV8-ATF3-ATF3$^{-/-}$ mice. The total area as the area under the curve (AUC) expressed as arbitrary units (AU) in **E** and **G**. The bar graph inset in panels **D** and **F** shows the contraction of 5-HT at each dose application. Overlap the total area profiles in both groups for comparison (**H**). Quantification data from panel **H** is expressed as Δabc in panel **I**. Statistical comparisons between two groups were performed by unpaired t-test (**E, G,** and **I**) and two-way ANOVA was performed in **B** and **C**). Data are presented as mean ± standard error of the mean (SEM). *$p < 0.05$, compared to the AAV8-GFP-ATF3$^{-/-}$group in each experiment. #There is a statistically significant difference among these sets of curves by the generalized estimating equation (GEE) analysis. The dotted symbols in each column represent the number of mice examined.

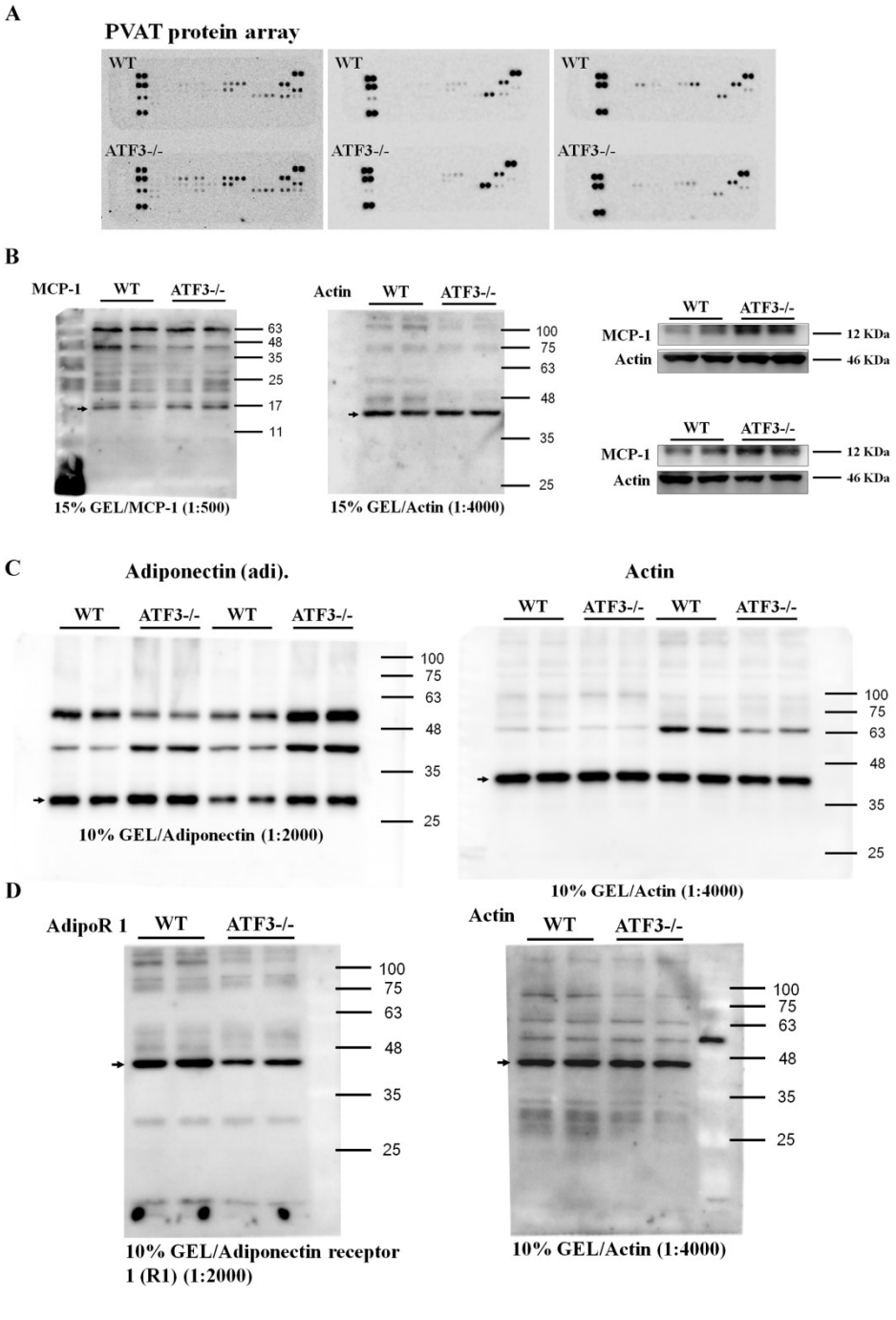
A
PVAT protein array
WT
ATF3-/-
B
MCP-1
Actin
15% GEL/MCP-1 (1:500)
15% GEL/Actin (1:4000)
12 KDa
46 KDa
C
Adiponectin (adi).
Actin
10% GEL/Adiponectin (1:2000)
10% GEL/Actin (1:4000)
D
AdipoR 1
10% GEL/Adiponectin receptor 1 (R1) (1:2000)
10% GEL/Actin (1:4000)
E
Adi.
30 KDa
43 KDa
46 KDa

Figure S8. Additional examples of representative images shown in the main and supplementary figures, related to Figure 8.

Protein levels of MCP-1, C-reactive protein, IL-6, resistin, PAI-1, and adiponectin in PVAT (n = 6 per group) after wild-type (WT) and ATF3$^{-/-}$mice 22 weeks HFD feeding by adipokine assays (**A**). The Image J Analyzer software was used for densitometry of blots (**A**). Representative images shown that MCP-1 protein level in thoracic aortic PVAT of wild-type and ATF3$^{-/-}$ mice (n = 6 per group) after HFD feeding for 22 weeks (**B**). Representative images shown that adiponectin protein level in thoracic aortic PVAT of wild-type and ATF3$^{-/-}$ mice after HFD feeding for 22 weeks (**C**). Adiponectin receptor 1 (adipoR1) protein level in thoracic aortic PVAT of wild-type and ATF3$^{-/-}$ mice after HFD feeding for 22 weeks (**D**). Adiponectin and adipoR1 protein levels in thoracic aortic PVAT of wild-type and ATF3$^{-/-}$ mice after HFD feeding for 22 weeks (**D**) in different experiments (n = 12 per group). Actin serves as internal control.